Available online at www.sciencedirect.com
SCIENCE DIRECT®
Journal of Magnetic Resonance 161 (2003) 43–55
JMR Journal of Magnetic Resonance
www.elsevier.com/locate/jmr

Multiple-quantum magic-angle spinning spectroscopy using nonlinear sampling

David Rovnyak,[a,c] Claudiu Filip,[a,b] Boris Itin,[a,b] Alan S. Stern,[d] Gerhard Wagner,[a,c] Robert G. Griffin,[a,b] and Jeffrey C. Hoch[d,*]

[a] *MIT/Harvard Center for Magnetic Resonance, Massachusetts Institute of Technology, 150 Albany Street, Cambridge, MA 02139, USA*
[b] *Department of Chemistry, Massachusetts Institute of Technology, 150 Albany Street, Cambridge, MA 02139, USA*
[c] *Department of Biological Chemistry and Molecular Pharmacology, Harvard Medical School, 240 Longwood Avenue, Boston, MA 02115, USA*
[d] *Rowland Institute for Science, 100 Edwin H. Land Boulevard, Cambridge, MA 02142, USA*

Received 8 July 2002; revised 10 December 2002

Abstract

NMR spectroscopy is a relatively insensitive technique and many biomolecular applications operate near the limits of sensitivity and resolution. A particularly challenging example is detection of the quadrupolar nucleus ^{17}O, due to its low natural abundance, large quadrupole couplings, and low gyromagnetic ratio. Yet the chemical shift of ^{17}O spans almost 1000 ppm in organic molecules and it serves as a potentially unique reporter of hydrogen bonding in peptides, nucleic acids, and water, and as a valuable complement to ^{13}C and ^{15}N NMR. Recent developments including the multiple-quantum magic-angle spinning (MQMAS) experiment have enabled the detection of ^{17}O in biological solids, but very long data acquisitions are required to achieve sufficient sensitivity and resolution. Here, we perform nonlinear sampling in the indirect dimension of MQMAS experiments to substantially reduce the total acquisition time and improve sensitivity and resolution. Nonlinear sampling prevents the use of the discrete Fourier transform; instead, we employ maximum entropy (MaxEnt) reconstruction. Nonlinearly sampled MQMAS spectra are shown to provide high resolution and sensitivity in several systems, including lithium sulfate monohydrate ($LiSO_4$-$H_2{}^{17}O$) and L-asparagine monohydrate ($H_2{}^{17}O$). The combination of nonlinear sampling and MaxEnt reconstruction promises to make the application of ^{17}O MQMAS practical in a wider range of biological systems.

Keywords: Oxygen-17; Quadrupolar nuclei; Nonlinear sampling; Maximum entropy reconstruction; MQMAS; Multi-dimensional NMR

1. Introduction

Quadrupolar nuclei comprise more than 60% of the periodic table and assume a rich variety of structural and functional roles in the molecular biology of living organisms [1,2]. Direct NMR observation of their quadrupole and chemical shift parameters provides insight into local electronic structure and geometry. Quadrupoles can serve as site-specific reporters in key regions of biomolecular function, and progress in NMR methodology will advance our understanding of quadrupoles in the life sciences. Recent quadrupolar NMR studies in biological solids have reported cobalt and sodium NMR spectra [3–8], and significant progress is also being made with magnesium, oxygen, and zinc NMR [9–19]. Much of the recent progress in quadrupolar NMR is due to the introduction of the multiple-quantum magic-angle spinning (MQMAS) experiment, which is the only method capable of providing isotropic quadrupolar spectra with conventional magic-angle spinning (MAS) probes [20,21].

One of the most challenging quadrupolar nuclei to observe is ^{17}O due to its low natural abundance (0.037%), large quadrupole couplings ($e^2qQ/h = 4$–20 MHz), and low gyromagnetic ratio ($\gamma(^{17}O)/\gamma(^1H) \approx 0.14$). While quadrupolar nuclei are exquisitely sensitive reporters of molecular geometry [22], there are additional benefits for observing ^{17}O solid-state NMR spectra. They include the

* Corresponding author. Fax: 1-617-497-4627.
E-mail address: hoch@rowland.org (J.C. Hoch).

1090-7807/03/$ - see front matter © 2003 Elsevier Science (USA). All rights reserved.
doi:10.1016/S1090-7807(02)00189-1

chemical shift dispersion of ^{17}O, which spans almost 1000 ppm in organic molecules [23,24], and the sensitivity of quadrupole and chemical shift parameters to hydrogen bonding [23,25–28]. Whether in amino acids, nucleotides, or water molecules, oxygen witnesses or participates in nearly all biological processes and has the potential to become as valuable to NMR-based biological studies as ^{13}C and ^{15}N.

The acquisition of solid-state ^{17}O NMR spectra in small biological molecules is feasible, but the methodology is not yet routine [12–17,26,27,29,30]. It was previously shown that high isotopic enrichment, fast magic-angle spinning, rotor-synchronized acquisition [31], and high radio-frequency power levels were crucial to the observation of ^{17}O 3Q-MQMAS spectra in several phosphates and hydrates [30]. Further enhancements are needed to study larger biomolecules and to observe larger quadrupole couplings. Recoupling methods, for example, are now commonly applied to systems where sensitivity is favorable (e.g., ^{23}Na, ^{27}Al, ^{11}B, ^{87}Rb), but the low sensitivity of ^{17}O NMR does not allow for such extensions at present. Moreover, several sensitivity enhancement schemes that are available in quadrupolar NMR are not practical for ^{17}O NMR. For example, rotation-induced adiabatic coherence transfer (RIACT) only effects useful coherence transfers between the central transition and the 5Q coherence in $S = 5/2$ systems [32]; it was not used in the present study since scaled dipolar couplings in 5Q-MQMAS of proton-coupled species can result in rapid loss of 5Q coherence. Also, short relaxation times and the difficulty of applying high-power decoupling for concatenated acquisitions prohibit the use of echo trains to improve sensitivity [33,34].

NMR experiments on quadrupolar nuclei encounter several challenging problems. For example, nearly degenerate lines may arise in MQMAS spectra when chemical shift dispersion is small (e.g., ^{23}Na), when measuring J couplings [35], or when observing asymmetric doublets from residual dipolar couplings [36,37]. Long evolution times are required to resolve these lines. On the other hand, many multi-dimensional experiments give rise to quadrupole-broadened resonances. These include MQMAS, heteronuclear correlation [38,39], homonuclear dipolar recoupling [40], exchange spectroscopy [4,41], nutation spectroscopy [3,4], and a rapidly growing list of other recoupling methods [36,37,42,43]. Finally, large quadrupole couplings, low natural abundances, and low gyromagnetic ratios can result in substantially reduced sensitivity.

To attack these problems we have applied nonlinear sampling combined with maximum entropy reconstruction (MaxEnt). Nonlinear sampling means acquiring data at long evolution times without also acquiring data at all intervening integral multiples of the dwell time. With this technique high resolution can be achieved in much shorter experiment times. Advantages of MaxEnt include the fact that it makes no assumptions regarding the number or type of resonances and can handle arbitrary lineshapes. In addition, MaxEnt has been shown to robustly handle data with low S/N ratios [44]. For a review of MaxEnt and other methods for handling truncated or incomplete acquisitions, see [45] and sources therein. Recently, the filter diagonalization method (FDM) has been utilized to shorten indirect acquisition times in n-D NMR of proteins [46,47], and a time-domain fitting technique using prior knowledge of resonance frequencies and Lorentzian linewidths (ANAFOR) [48] has been applied in MQMAS spectroscopy. However, both of these methods assume Lorentzian line shapes and thus are not as generally suited for application to solid-state NMR.

We applied MaxEnt to obtain ^{17}O 3Q-MQMAS spectra of several samples, including L-asparagine-$H_2{}^{17}O$, using exponential sampling schedules for the indirect dimension. Time-savings of factors of 2–4 are realized without any loss of resolution or sensitivity. In some experiments, the time saved was used for additional signal averaging to improve the sensitivity of ^{17}O MQMAS spectra of species with large quadrupole couplings. Our results show that the combination of MaxEnt and nonlinear sampling is a robust and powerful, albeit underutilized, methodology for extending the resolution and sensitivity limits of the MQMAS experiment.

2. Maximum entropy reconstruction

The theory of MaxEnt reconstruction has been described in detail elsewhere [45,49]; here we summarize the salient characteristics. In contrast to the discrete Fourier transform (DFT), which computes the spectrum directly from the measured data, MaxEnt reconstructs a spectral estimate by finding among all the spectra that are consistent with the experimental data the one having the highest entropy. In practice, this means that a spectrum $\mathbf{f}$ is accepted as consistent with the experimental data $\mathbf{d}$ when the mismatch between $\mathbf{d}$ and the inverse DFT of $\mathbf{f}$ (the mock data $\hat{\mathbf{d}}$) is comparable to the amount of noise, C_0, estimated to be contained in the experimental data. C_0 can be estimated from the tail of an FID or from an FID in a portion of the data that contains no signal. This constraint is expressed as

$$C(\mathbf{f},\mathbf{d}) \leqslant C_0, \tag{1a}$$

where $C(\mathbf{f},\mathbf{d})$ is the unweighted χ^2 statistic,

$$C(\mathbf{f},\mathbf{d}) = \sum_{i=0}^{M-1} |\hat{d}_i - d_i|^2, \tag{1b}$$

where M is the number of experimental data points. In general there are infinitely many spectra that are con-

sistent with any **d**. MaxEnt reconstruction yields the unique spectrum that is the solution to the constrained optimization

$$\text{Maximize } S(\mathbf{f}) \quad \text{subject to } C(\mathbf{f},\mathbf{d}) \leqslant C_0,$$

where $S(\mathbf{f})$ is an appropriate entropy functional.

The subscript in Eq. (1b) uses only a single index, but it can easily be generalized to multiple dimensions. In addition, the sum in Eq. (1b) need not run over a contiguous range of indices. With nonlinear sampling, only the points that are actually collected contribute toward the sum. This raises the question of which sample points to collect. By analogy with the concept of the matched filter [50], the density of sampled points should be proportional to the signal intensity. For a Lorentzian signal, this means the sample density should decrease exponentially [51]; an exponential sampling schedule is a list of sample times having this distribution. For non-Lorentzian or non-decaying signals, other sampling schedules are more appropriate [52]. In practice, we find that it is not necessary to exactly match the sampling characteristics to the signal decay in order to obtain useful results. Just as a single linear filter can be used on data containing heterogeneous line shapes, a single sampling schedule can also be used to advantage in such circumstances.

The application of the maximum entropy principle to signal reconstruction was based originally on the Shannon entropy [53]

$$S(\mathbf{f}) = -\sum_{n=0}^{N-1} f_n \log f_n \tag{2a}$$

as the measure of the amount of missing information, where N is the number of points in the spectral estimate. The Shannon entropy formula is not applicable to spectra that are complex or contain negative (or zero) components. A number of modifications to the Shannon entropy to deal with complex, non-positive spectra have been proposed [54]; the functional [54,55],

$$S(\mathbf{f}) = -\sum_{n=0}^{N-1} \frac{|f_n|}{\text{def}} \times \log\left(\frac{|f_n|/\text{def} + \sqrt{4+|f_n|^2/\text{def}^2}}{2}\right) - \sqrt{4+|f_n|^2/\text{def}^2}, \tag{2b}$$

where def is a scale factor, was shown to yield the spectrum consistent with the maximum entropy distribution of an ensemble of spin-1/2 particles. In principle def is related to the spectrometer sensitivity, although it is generally treated as an adjustable parameter. Empirically, its value affects the signal level at which MaxEnt reconstructions become highly nonlinear [56], and it should be set to a value slightly above the peak noise amplitude and below that of the weakest signal component. We are concerned here with spectra for quadrupolar (i.e., spin $> 1/2$) particles and so there is some question whether Eq. (2b) is an appropriate functional. However, the experiments described here detect only the central transition of half-integer quadrupolar nuclei, and for MQMAS, the net isotropic evolution can be treated in an effective spin-1/2 subspace (see Eq. (11)). Thus we feel amply justified in using Eq. (2b) for the entropy functional. On a more practical level, functional (2b) was shown to be the simplest modification of the Shannon entropy that is insensitive to phase, strictly convex, and continuously differentiable on the complex plane [54]. In practice, it yields results quite similar to the Shannon entropy of the absolute magnitude spectrum.

The constrained optimization is converted to an equivalent unconstrained optimization through the introduction of a Lagrange multiplier, λ, to construct an objective function $Q(\mathbf{f},\mathbf{d}) = S(\mathbf{f}) - \lambda C(\mathbf{f},\mathbf{d})$. The maximum of $Q(\mathbf{f},\mathbf{d})$ is determined numerically. In the present work, we employ the constant-λ algorithm [45,57,58] implemented in the Rowland NMR Toolkit [49]; related algorithms and implementations are found in the programs GIFA [59], NMRPipe [60], and Azara [61].

Maximizing $Q(\mathbf{f},\mathbf{d})$ can be computationally intensive. This is particularly true for multi-dimensional processing where $\mathbf{f} = \mathbf{f}(t_1,t_2)$. However a row-wise, constant-λ algorithm provides equivalent results in a fraction of the time [58]. For example, reconstructions of the 2D-MQMAS spectra acquired in this study typically consumed about 10 s or less on an SGI O^2 workstation with one MIPS R5000 processor and 128 MB RAM.

The spectral estimates obtained using MaxEnt reconstruction are nonlinear functions of the input [56]. The values of the parameters def and C_0 determine the extent of the nonlinearity. While MaxEnt reconstruction is often described as yielding the spectrum that contains the least amount of information consistent with the data, we take the more utilitarian view that the entropy regularizer yields smooth spectral estimates that have appropriate asymptotic properties. In the limit where the weight applied to the constraint (λ) is so small that $Q(\mathbf{f},\mathbf{d})$ is dominated by the entropy, MaxEnt yields a blank, featureless spectrum. When the weight is much larger so that $Q(\mathbf{f},\mathbf{d})$ is dominated by the experimental constraint, the spectral estimate approaches the DFT of the data (provided that N is equal to M).

3. Theory

We review the MQMAS experiment [20,21], which creates an effective evolution period free of quadrupolar anisotropy, and derive expressions for the isotropic line positions in MQMAS spectra. The isotropic evolution

period consisting of N linear samples spans an effective evolution time $\tau_1^{(\mathrm{MQMAS})} = N(1+k)\Delta t_1$ and gives a spectral width upon Fourier transformation of $sw^{(\mathrm{MQMAS})} = [(1+k)\Delta t_1]^{-1}$, where Δt_1 is the time increment used in the pulse sequence (see Fig. 1 and the experimental section) and k is a constant to be determined later. The quadrupolar Hamiltonian in irreducible spherical tensor operator notation [62] is

$$H^{(Q)}(\mathrm{PAS}) = \omega_Q \sum_m R_{2m}^{(\mathrm{PAS})} T_{2,-m}, \tag{3}$$

where $\omega_Q = e^2qQ/\hbar 2I(2I-1)$ is the quadrupole coupling frequency. The spatial tensor components encode the asymmetry, η, and are expressed in a laboratory frame which is related to the principal axes system (PAS) by a set of Euler angles (α, β, γ) [63]:

$$\begin{aligned}
R_{20} &= \sqrt{\frac{3}{8}}\left[3\cos^2\beta - 1 + \eta\sin^2\beta\cos 2\alpha\right],\\
R_{2\pm1} &= \frac{1}{2}\sin\beta e^{\mp i\gamma}[\pm(3-\eta\cos 2\alpha)\cos\beta - i\eta\sin 2\alpha],\\
R_{2\pm2} &= \frac{1}{2}e^{\mp 2i\gamma}\left[\frac{3}{2}\sin^2\beta + \frac{\eta}{2}(1+\cos^2\beta)\cos 2\alpha \pm i\eta\cos\beta\sin 2\alpha\right].
\end{aligned} \tag{4}$$

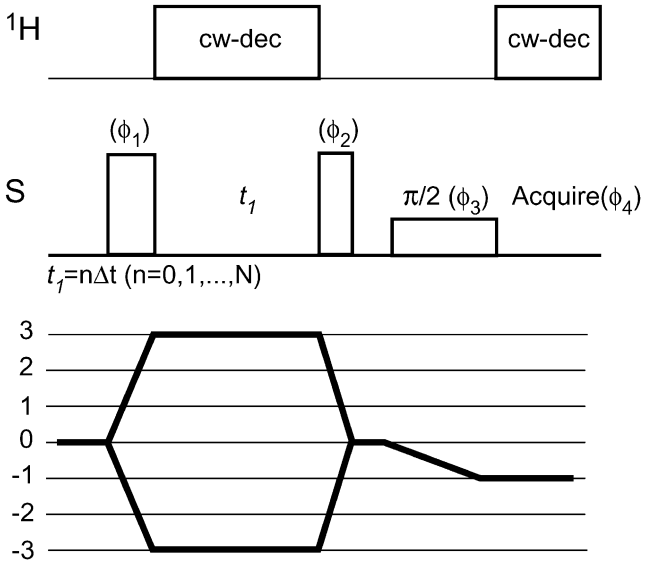

Fig. 1. Pulse sequence and coherence level transfer diagram for the phase-sensitive two-dimensional MQMAS experiment. The experiment is repeated with a 30° increment in the phase of the first pulse and processed via the hypercomplex method [99]. One strong pulse creates triple-quantum (3Q) coherence and is followed by the indirect evolution period, denoted t_1. A second strong pulse converts the 3Q coherence to central-transition polarization, which is followed by a short delay to allow transverse components to dephase (z-filter). Finally, a soft 90° pulse is applied to read out the FID. Phase cycling of the pulses is $\{\phi_1 = 0,0,60,60,120,120,180,180,240,240,300,300\}, \{\phi_2 = 0\}, \{\phi_3 = 0,180\}, \{\phi_4 = 0,180,180,0\}$.

The spin tensor components are

$$\begin{aligned}
T_{20} &= \frac{1}{\sqrt{6}}(3\mathbf{I_Z^2} - I(I+1)),\\
T_{2,\pm1} &= \mp\frac{1}{2}(\mathbf{I_Z}\mathbf{I}_\pm + \mathbf{I}_\pm\mathbf{I_Z}), \quad T_{2,\pm2} = \frac{1}{2}\mathbf{I}_\pm^2.
\end{aligned} \tag{5}$$

One may compute perturbations upon the Zeeman interaction [64], or determine corrections with average Hamiltonian theory [65]. Both yield identical secular terms. The low order term is $H_Q^{(0)} = R_{20}T_{20}$ and the next correction is

$$H_Q^{(1)} = \frac{\omega_Q^2}{2\omega_0}\sum_{m=\pm1,\pm2}\frac{1}{m}R_{2,m}R_{2,-m}[T_{2,m}, T_{2,-m}]. \tag{6}$$

Tensor products can be expressed in an expanded basis [66]. Thus

$$H_Q^{(1)} = \frac{\omega_Q^2}{\omega_0}\sum_{l=0}^{4}A_{l0}\left(C(22l;1,-1)[T_{2,1}, T_{2,-1}] + \frac{1}{2}C(22l;2,-2)[T_{2,2}, T_{2,-2}]\right), \tag{7}$$

where $C(l_1l_2l; m_1m_2)$ are Clebsch–Gordon coefficients (see also Table 1). Using

$$\mathbf{I_Z} = \sum_{m=\frac{1}{2},\frac{3}{2},\ldots,S} 2m\mathbf{I_Z^{m,-m}}$$

to introduce fictitious spin-1/2 operators, we find [67]

$$\begin{aligned}
H_Q^{(1)} &= \frac{\omega_Q^2}{\omega_0}\sum_{l=0,2,4}\sum_{m=\frac{1}{2},\ldots,S} C_{l,m}(S)A_{l,0}\mathbf{I_Z^{m,-m}},\\
C_{l,m}(S) &= \left(a_m^{(1)}(S)C(22l;1-1) + a_m^{(2)}(S)C(22l;2-2)\right),\\
a_m^{(1)}(3/2) &= -2m[4m^2-7],\\
a_m^{(1)}(5/2) &= -2m(4m^2-17),\\
a_m^{(2)}(3/2) &= -\frac{1}{2}m[4m^2-13],\\
a_m^{(2)}(5/2) &= -\frac{1}{2}m(4m^2-33),
\end{aligned} \tag{8}$$

Table 1
Spin tensor commutation relationships for $S = 3/2$ and $S = 5/2$ nuclei, obtained using the methods of Refs. [100,101]. Note that the commutators depend linearly on $\mathbf{I_Z}$ through T_{10}, which leads to second-order broadening of any symmetric transition

	$S = 3/2$	$S = 5/2$
$[T_{21}, T_{2,-1}]$	$-\frac{6}{5}T_{10} - 4\sqrt{\frac{2}{5}}T_{30}$	$-\frac{16}{5}T_{10} - 4\sqrt{\frac{2}{5}}T_{30}$
$[T_{22}, T_{2,-2}]$	$\frac{12}{5}T_{10} - 2\sqrt{\frac{2}{5}}T_{30}$	$\frac{32}{5}T_{10} - 2\sqrt{\frac{2}{5}}T_{30}$
$T_{10} = \mathbf{I_Z}$	$T_{30} = \sqrt{\frac{1}{10}}[5\mathbf{I_Z^3} - (3I(I+1)+1)\mathbf{I_Z}]$	

where the central-transition or triple-quantum subspaces may be described by setting $m = 1/2$ or $m = 3/2$, respectively, and the A_{lm} are the laboratory frame tensor components in the new basis [65]. In the PAS, they are

$$\begin{aligned}
&\rho_{00} = \frac{(3+\eta^2)}{2\sqrt{5}}, \quad \rho_{20} = -\frac{(3-\eta^2)}{\sqrt{14}},\\
&\rho_{2\pm1} = 0, \quad \rho_{2\pm2} = \sqrt{\frac{3}{7}}\eta,\\
&\rho_{40} = \frac{\left(9+\frac{1}{2}\eta^2\right)}{\sqrt{70}}, \quad \rho_{4\pm1} = 0,\\
&\rho_{4\pm2} = \frac{3}{2\sqrt{7}}\eta, \quad \rho_{4\pm3} = 0, \quad \rho_{4\pm4} = \frac{1}{4}\eta^2,
\end{aligned} \tag{9}$$

where the ρ_{00} term indicates an isotropic contribution of the quadrupole coupling. For sample rotation about an angle θ, the space terms in Eq. (8) transform as Legendre polynomials. For the central transition, the time-independent terms are

$$\begin{aligned}
H^{(1)}_{Q,\mathrm{rot}} = \Big[&C_{0,\frac{1}{2}}(S)A_{00} + C_{2,\frac{1}{2}}(S)A_{20}P_2(\cos\theta)\\
&+ C_{4,\frac{1}{2}}(S)A_{40}P_4(\cos\theta)\Big]\mathbf{I}_{\mathbf{Z}}^{1/2,-1/2}.
\end{aligned} \tag{10}$$

The second- and fourth-order Legendre terms do not have a common node, so no single axis of rotation can remove the quadrupolar anisotropy. The MQMAS experiment solves this problem by correlating evolution of a symmetric, multiple-quantum coherence with evolution of central-transition coherence during magic-angle spinning. The fourth-order anisotropy ($l = 4$) is refocused in the acquisition period and MAS ($\theta = 54.74°$) removes $l = 2$ terms. Many coherence transfer methods exist [21,32,38,67–79] and the z-filtered, phase-sensitive experiment [80] used in this study is shown in Fig. 1. Phase accumulation due to the fourth-order term depends on the coherence order in each evolution period; thus the isotropic echo forms at a time $t_2 = kt_1$. An effective Hamiltonian for the evolution period, $\tau_1^{(\mathrm{MQMAS})} = (1+k)t_1$, is

$$\begin{aligned}
H^{(\mathrm{MQMAS})}_{Q,\mathrm{eff}} = \frac{1}{1+k}\Bigg[&\sum_{l=0,2}(2m+k)A^{\mathrm{CS}}_{l0}\\
&+ \sum_{l=0,2,4}\Big(kC_{l,\frac{1}{2}}(S)\\
&+ C_{l,m}(S)\Big)A^{Q}_{l0}\Bigg]\mathbf{I}_Z^{1/2,-1/2},
\end{aligned} \tag{11}$$

where $2m$ is the multiple-quantum coherence order and the chemical shift is $H^{\mathrm{CS}} = \sum_{l=0,2} 2mA_{l0}\mathbf{I}_{\mathbf{Z}}^{1/2,-1/2}$. The MQMAS condition, $kC_{4,1/2}(S) + C_{4,m}(S) = 0$, removes $l = 4$ terms and is satisfied for coherence orders (p) of the same sign for $S = 3/2$ ($p : 3 \to 1$) and of opposite sign for $S = 5/2$ ($p : -3 \to 1$). The constant k may be computed following equation (8). For 3Q-MQMAS of $S = 5/2$ nuclei, $k = 19/12$. Finally, we have

$$\begin{aligned}
\omega^{3Q}_{\mathrm{iso}}\left(S=\frac{3}{2}\right) &= \frac{2m+k}{1+k}\omega_{\mathrm{CS}} + \frac{9}{10}\left(\frac{3-k}{1+k}\right)\frac{\omega_Q^2}{\omega_{\mathrm{CS}}}\left(1+\frac{1}{3}\eta^2\right)\\
&= \left[\frac{17}{8} + \frac{9}{8}\frac{\omega_Q^2}{\omega_{\mathrm{CS}}^2}\left(1+\frac{1}{3}\eta^2\right)\right]\omega_{\mathrm{CS}},\\
\omega^{3Q}_{\mathrm{iso}}\left(S=\frac{5}{2}\right) &= \frac{-2m+k}{1+k}\omega_{\mathrm{CS}} + \frac{3}{5}\left(\frac{3-4k}{1+k}\right)\frac{\omega_Q^2}{\omega_{\mathrm{CS}}}\left(1+\frac{1}{3}\eta^2\right)\\
&= -\left[\frac{17}{31} + \frac{24}{31}\frac{\omega_Q^2}{\omega_{\mathrm{CS}}^2}\left(1+\frac{1}{3}\eta^2\right)\right]\omega_{\mathrm{CS}}.
\end{aligned} \tag{12}$$

Analysis of MQMAS line positions with Eq. (12) may be combined with numerical fits of MAS or static lineshapes to yield quadrupole and chemical shift parameters.

4. Results

We first examine spectra obtained by discrete Fourier transformation of truncated linearly sampled data and by MaxEnt reconstruction of nonlinearly sampled data. For linearly sampled data we used linear prediction (LP) to extend the datasets, which can introduce frequency bias and false signals [44], and which enhances resolution in the resulting spectra largely by eliminating sinc-wiggles that arise from Fourier transformation of incompletely sampled signals [45]. With low-to-medium S/N ratios, if a signal has been acquired for a time τ, then lines separated by less than $1/\tau$ in the frequency domain will not be resolved with the DFT, regardless of any data extension by LP extrapolation. This is demonstrated in the left-hand column of Fig. 2, in which successive truncations of an experimental, isotropic ^{17}O 3Q-MQMAS FID are processed by applying LP followed by the DFT. This approach does not resolve the closely spaced lines unless there are at least 96 t_1 samples ($\tau_1^{(\mathrm{MQMAS})} = 96(1+k)\Delta t_1 = 3.1\,\mathrm{ms}$) and it is evident that the resolution of MQMAS is constrained by the acquisition time in t_1. The resonances differ by 300 Hz and are only resolved by recording data up to $\tau_1^{(\mathrm{MQMAS})} = 3.3\,\mathrm{ms}$.

For nonlinearly sampled data, we used exponential sampling schedules for sampling t_1 sparsely without giving up information at long times [81,82]. MaxEnt reconstructions of exponentially sampled data taken from the full dataset are shown in the right-hand column of Fig. 2. Two lines are clearly resolved for all sampling schedules, which contain samples up to and including the final sample ($N = 145$) at $\tau_1^{(\mathrm{MQMAS})} = 4.7\,\mathrm{ms}$. Fourier transformation of the full FID indicates a S/N ratio of 20:1 and so the right-hand column of Fig. 2 confirms the ability of MaxEnt to faithfully reconstruct noisy data [44]. These data are relatively densely sampled in t_1

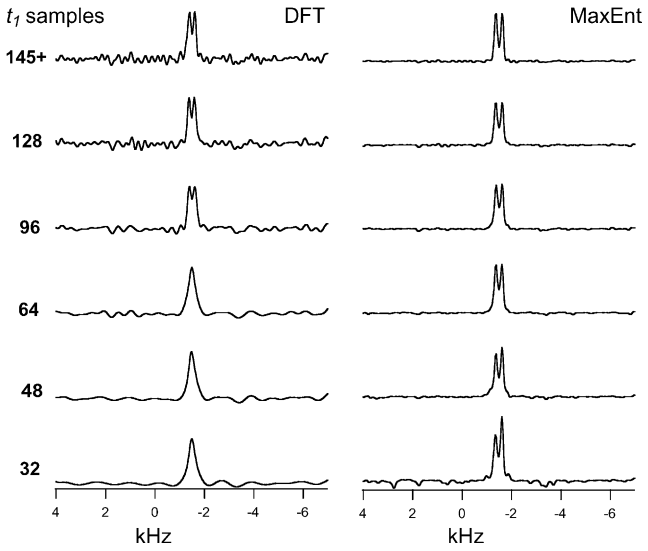

Fig. 2. Different processing schemes of the isotropic FID from a single ^{17}O 3Q-MQMAS spectrum which was sampled to an effective time $\tau_1^{(\mathrm{MQMAS})} = N(1+k)\Delta t_1 = 4.7\,\mathrm{ms}$, where $N = 145$ and $\Delta t_1 = 12.5\,\mu\mathrm{s}$. The left column shows spectra obtained by LP and Fourier transformation. Successive truncations are made by eliminating points from the end of the FID. The right column shows spectra obtained by MaxEnt reconstruction, where data reductions are made by selecting points according to exponential sampling schedules. All sets in the right column contain samples up to and including 4.7 ms.

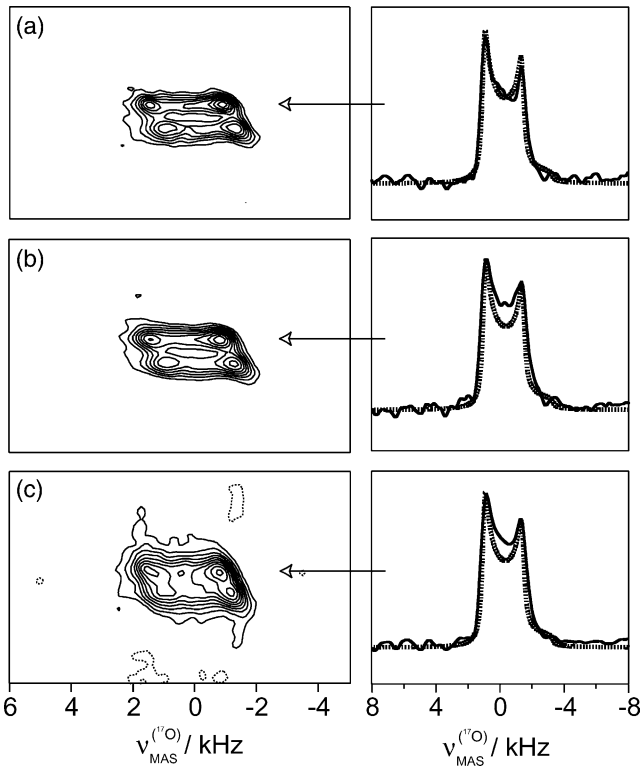

Fig. 3. Comparison of discrete Fourier transformation and MaxEnt reconstruction using a single pure absorption mode ^{17}O 3Q-MQMAS dataset of hydroxyapatite, $Ca_5(P^{17}O_4)_3(OH)$, acquired at 9.4 T with the pulse sequence of Fig. 1. The indirect dimensions consist of (a) linearly sampled t_1 points spanning $\tau_1^{(\mathrm{MQMAS})} = N(1+k)\Delta t_1 = 7.8\,\mathrm{ms}$ with $N = 60$ and $\Delta t_1 = 50.5\,\mu\mathrm{s}$ processed by double Fourier transformation, (b) 40 slices exponentially selected from the first data set processed by MaxEnt, and (c) 20 exponentially selected slices from the first data set processed by MaxEnt. The recycle time was 2 s and 528 transients were collected for the real and imaginary parts (1056 for each complex slice). A computed fit has been arbitrarily adjusted through line broadening to match the spectrum in (a) and is superimposed without modification onto the spectra in (b) and (c).

and only the isotropic FID was treated in Fig. 2. It is, however, common to use much longer t_1 intervals when the spectrum lies in a narrow spectral range. For example, rotor-synchronized MQMAS [31,83] requires increments proportional to the inverse of the rotor period. It is also useful to process pure absorption mode, two-dimensional MQMAS spectra, and we investigate these conditions next.

Pure absorption mode ^{17}O 3Q-MQMAS spectra of hydroxyapatite, acquired by the hypercomplex z-filter method [80] and using rotor-synchronization, are shown in Fig. 3, where the indirect dimension was acquired with 60 samples spanning $\tau_1^{(\mathrm{MQMAS})} = 7.8\,\mathrm{ms}$. Conventional Fourier transformation of the full linearly sampled dataset is shown in Fig. 3a along with a representative f_1 cross-section (slice) and numerical fit. Contours are plotted starting at 10% of the maximum intensity and up in steps of 10% for all spectra. MaxEnt processing of the dataset after selecting 40 t_1 values with exponentially increased spacings is shown in Fig. 3b. The contour plot verifies that the constant-λ algorithm provides pure-phase 2D-MQMAS spectra. MaxEnt processing after exponentially selecting 20 t_1 slices is shown in Fig. 3c. Again the contour plot and the slice are both in excellent agreement with Fig. 3a; however, the appearance of some low intensity negative artifacts, similar to those observed in the bottom MaxEnt reconstruction in Fig. 2, indicates that further truncation is not advisable. In our hands this set could be truncated even to 15 slices; however, this required more careful tuning of MaxEnt parameters, Gaussian apodization, and phasing, whereas the use of 20 slices required no such effort. Figs. 3b and c were obtained by extracting samples from the full dataset used in Fig. 3a. The slight discrepancy between the simulated spectrum and the data in Figs. 3b and c is due to arbitrarily adjusting the simulation with slight line broadening to superimpose with Fig. 3a. More generally, relaxational anisotropy often complicates lineshape analysis in quadrupolar NMR, and it is most important to observe in Fig. 3 the excellent agreement between the singularities in the simulated and MaxEnt reconstructed spectra. If the nonlinear sampling schemes of Figs. 3b and c were experimentally implemented, the measurement time would be reduced by factors of 1.5 and 3.0, respectively.

A principal goal of this study is to investigate the use of nonlinear sampling to obtain improved sensitivity in MQMAS spectroscopy. In this case we consider a simpler

two-pulse nutation approach [21,67,84] that would be obtained by removing the soft 90° pulse in Fig. 1 and changing the phase cycling to select for the $\mathbf{I}_Z \rightarrow 3Q \rightarrow 1Q$ pathway. The reason for this is the non-ideal response of half-integer quadrupolar nuclei to RF irradiation in powdered solids [70,85–87]. The effective nutation rate depends upon crystallite orientation in a manner that becomes increasingly severe with increasing quadrupole coupling. This effective RF inhomogeneity can result in significant signal losses, such that MQMAS sequences with the fewest pulses tend to produce the best sensitivity for samples with very large quadrupole couplings. We note also that 2D-MQMAS spectra acquired without pure-phase methodology can still retain a relatively high degree of absorptive character [68,88]. While sensitivity considerations do not exclude using a sequence such as Fig. 1, the two-pulse nutation approach is more sensitive for acquiring MQMAS spectra of oxygen-^{17}O samples with large quadrupole couplings. A comparison of coherence transfer methods in spin-5/2 nuclei [74,76,89] and phase-sensitive sequences [88] for ^{17}O 3Q- and 5Q-MQMAS NMR is outside the scope of this work.

We demonstrate in Fig. 4 the use of nonlinear sampling to improve sensitivity with a series of ^{17}O 3Q-MQMAS spectra of ammonium dihydrogen phosphate (ADP, $NH_4H_2P^{17}O_4$), acquired with the two-pulse method. The first row shows linearly sampled data acquired with 48 t_1 slices spanning $\tau_1^{(\mathrm{MQMAS})} = 6.2$ ms, with 1800 transients per increment. The second and third rows show exponentially sampled data with 24 and 16 t_1 slices and 3600 and 5400 transients per slice, respectively. Due to the nonlinearity of MaxEnt reconstruction, the improvement in sensitivity is best appreciated by comparing representative slices of the raw time-domain echo signals. For example the fourth t_1 slice is used in both exponential sampling schedules and is shown in the first column of Fig. 4, where the improvement in sensitivity is apparent. In the middle column, the two-dimensional spectra are shown with contours plotted at 15% of the maximum intensity in steps of 10%. As in Fig. 3, consistent lineshapes are obtained for the linear and exponentially sampled experiments, demonstrating again that MaxEnt reconstruction along f_1 correctly reproduces information in f_1 and f_2. Finally, MaxEnt reconstructions of the isotropic FIDs are shown in the third column, where all three spectra are again found to be in excellent agreement. Some non-Lorentzian line broadening can be seen near the baseline of the f_1 dimension for the highly truncated spectra in Figs. 3 and 4. This behavior depends upon the

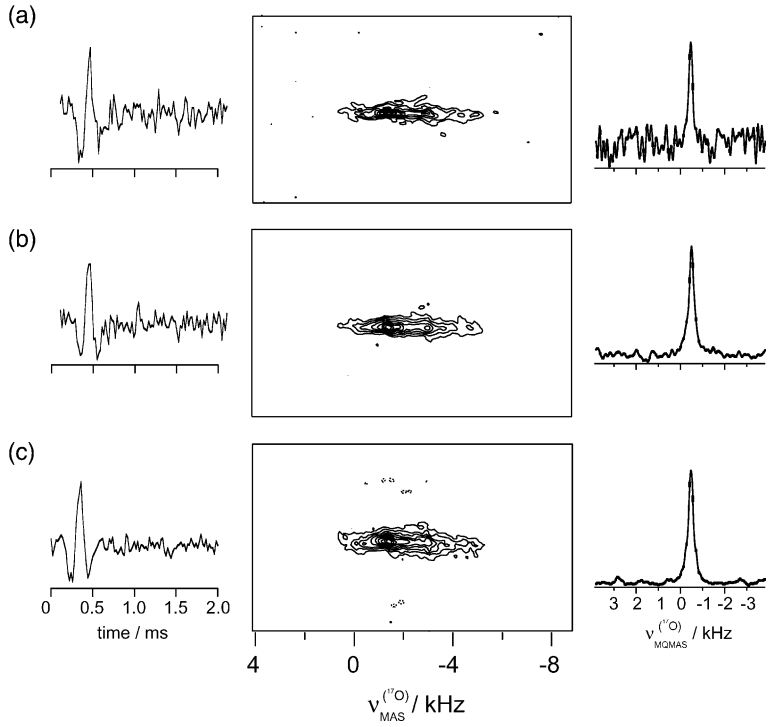

Fig. 4. Comparison of 2D-^{17}O-3Q-MQMAS spectra for ammonium dihydrogen phosphate ($NH_4H_2P^{17}O_4$), acquired with a two-pulse method obtained by eliminating the z-filter in Fig. 1. Linearly sampled (a) and nonlinearly sampled (b,c) datasets were acquired separately. Spectra in row (a) are from $N = 48$ linear samples spanning $\tau_1^{(\mathrm{MQMAS})} = N(1+k)\Delta t_1 = 6.2$ ms with $\Delta t_1 = 50.5\,\mu$s and 1800 transients per slice and are processed by Fourier transformation. Spectra in rows (b) and (c) are from 24 and 16 exponentially selected t_1 samples with 3600 and 5400 transients per slice, respectively, and are processed by MaxEnt. The recycling time was 0.5 s and each experiment required 12 h. The first column shows the time-domain data sampled at $\tau_1^{(\mathrm{MQMAS})}(N=4) = 4(1+k)\Delta t_1 = 0.39$ ms. The middle column shows the result of sheared, two-dimensional processing where contours for all three spectra are plotted at 15% in steps of 10% of the maximum intensity. The final column displays MaxEnt reconstructions of the isotropic FID for each acquisition.

quality of data at long evolution times and will be considered further in the discussion.

We next demonstrate the use of MaxEnt reconstruction and exponential sampling to obtain well-resolved MQMAS spectra of ^{17}O-enriched compounds with large quadrupole coupling constants. Previously, we reported an ^{17}O 3Q-MQMAS spectrum of barium chlorate monohydrate that was isotopically enriched in the water position ($e^2qQ/h = 6.8$ MHz, $\eta = 1.0$) [30]. This spectrum suffered from severe truncation artifacts since time was invested in acquiring sufficient transients for a small number of linearly sampled t_1 increments. Low sensitivity and the small number of slices prevented the use of LP. In contrast, MaxEnt reconstructions of exponentially sampled experiments should provide satisfactory results. We chose two samples enriched with ^{17}O (74%) in the water molecules and which possess large quadrupole couplings to test this prediction: lithium sulfate monohydrate and L-asparagine monohydrate. Static and MAS experiments in our laboratory indicated that the ^{17}O quadrupole coupling parameters for the water of lithium sulfate are $e^2qQ/h = 6.8$ MHz and $\eta = 1.0$. For L-asparagine monohydrate, the quadrupole coupling parameters of the water site had been indirectly estimated at $e^2qQ/h = 7.6$ MHz and $\eta = 1.0$ [90]. An additional reason for choosing L-asparagine is that previous attempts to acquire linear ^{17}O 3Q-MQMAS spectra of L-asparagine monohydrate (unpublished results) were unsatisfactory due to the difficulty of obtaining a sufficiently high S/N ratio and enough t_1 samples to avoid truncation artifacts. Crystal structures report one crystallographically distinct water molecule per unit cell in both samples [91,92]; however, it has been speculated that the six water molecules in the L-asparagine unit cell may be inequivalent [90].

MaxEnt reconstructions of isotropic 3Q-MQMAS experiments are shown for L-asparagine monohydrate in Fig. 5a and lithium sulfate monohydrate in Fig. 5b. In each experiment, 16 samples have been distributed over $\tau_1^{(\mathrm{MQMAS})} = 6.2$ ms. We observe only one line for L-asparagine monohydrate. We also record a single line for lithium sulfate monohydrate. We have determined the ^{17}O quadrupole coupling parameters in L-asparagine monohydrate to be $e^2qQ/h = 7.0$ MHz and $\eta = 1.0$, which is a slight downward revision of the previous estimates [90].

The sensitivity of the L-asparagine experiment is poorer compared to the lithium sulfate spectrum. This is due in part to the slightly larger quadrupole coupling, since nutation efficiencies decrease rapidly even for small increases in quadrupole couplings [21,32,67,68]. L-asparagine also has a higher proton density introducing more dipolar couplings, which are scaled by 3 in the 3Q evolution period, and which also enhance relaxation. An additional problem is that the crystal cell of L-asparagine may dehydrate under rapid sample spinning. Care

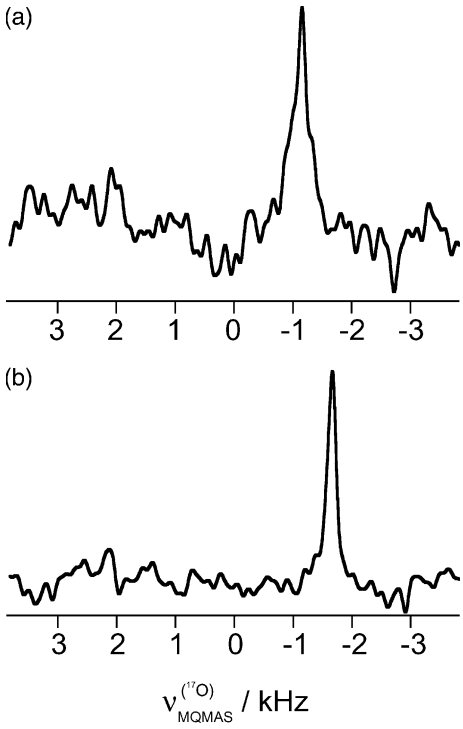

Fig. 5. MaxEnt reconstructions of nonlinearly sampled isotropic MQMAS FIDs for (a) L-asparagine monohydrate ($H_2{}^{17}O$, 74%-^{17}O) and (b) lithium sulfate monohydrate ($H_2{}^{17}O$, 74%-^{17}O). The L-asparagine spectrum was acquired with $N = 16$ exponentially distributed slices spanning $\tau_1^{(\mathrm{MQMAS})} = N(1+k)\Delta t_1 = 6.2$ ms, with 12,000 transients per slice. The lithium sulfate spectrum was acquired with $N = 16$ slices spanning $\tau_1^{(\mathrm{MQMAS})} = 6.2$ ms, with 14,400 transients per slice. For (a) and (b) a two-pulse MQMAS sequence was used by eliminating the z-filter from Fig. 1. A recycle time of 1 s was used.

was taken to seal the rotor containing L-asparagine monohydrate, since significant signal losses and spectral degradation were noted in tests with unsealed rotors. Thus, we infer that we observed the portion of the sample with hydrated unit cells, which would correspond to the central core of the rotor where centripetal forces are weaker. The isotropic MQMAS linewidths at half-height are 240 and 160 Hz for L-asparagine and lithium sulfate, respectively.

The isotropic chemical shift and quadrupolar coupling terms for all samples used in this study are summarized in Table 2 and were obtained by comparing

Table 2
Quadrupole and isotropic chemical shift parameters for the compounds in this study. Isotropic shifts are referenced to a sample of liquid $H_2{}^{17}O$ (30% ^{17}O) and errors are estimated to be ±2 ppm. Errors for e^2qQ/h and η are estimated at 0.05 MHz and 0.05, respectively

Sample	Peak	e^2qQ/h (MHz)	η	δ_{iso} (ppm)
$Ca_5(P^{17}O_4)_3(OH)$	1	4.2	0.0	118
	2	4.3	0.0	111
$NH_4H_2P^{17}O_4$		5.2	0.6	92.8
Li_2SO_4-$H_2{}^{17}O$		6.8	0.9	0.5
L-Asparagine-$H_2{}^{17}O$		7.0	1.0	7.0

isotropic MQMAS line positions with simulations of MAS powder lineshapes. In the cases of lithium sulfate monohydrate and L-asparagine monohydrate, static echo-detected experiments were also acquired to provide additional confirmation of these parameters.

5. Discussion

As this work is the initial application of MaxEnt reconstruction and nonlinear sampling to solid-state NMR data, the first goal of the study was to establish the fidelity of the methodology and guidelines for acceptable truncation limits. It is clear from Figs. 2–4 that spectral information in f_1 and f_2 is consistently reproduced by MaxEnt with datasets truncated by factors of 2–4. We have also confirmed the ability of MaxEnt reconstruction to handle pure absorption phase, two-dimensional experiments, which has already been demonstrated in liquid-state spectroscopy [45]. We find that eliminating sampling points by factors of 2–3 is advisable if a long dwell time in t_1 would allow for satisfactory resolution with a moderate number of linear samples as in Figs. 3–5, or if signal-to-noise ratios are low. Eliminating sampling points by factors of 3–4 is advisable if a short dwell time in t_1 would dictate acquiring a large number of linear samples, as in Fig. 2, and when sensitivity is high. An experienced user may extend these limits, but routine application of nonlinear sampling and MaxEnt methodology should adhere to these guidelines.

The second goal was to investigate the sensitivity limits of MQMAS NMR when the time-savings from reduced sampling is fully invested in increasing the number of transients collected per slice. In samples with very large quadrupole couplings, the number of transients needed to obtain echoes that are measurably distinct from the noise means that 3–4 h or more are needed to acquire each slice. If linear sampling is used, then severe truncation effects can result, as evidenced in a previous spectrum of barium chlorate at 9.4 T ($e^2qQ/h = 6.8$ MHz, $\eta = 1.0$) [30]. Elimination of such truncation artifacts with LP is often not practical due to the low S/N and the short overall acquisition time in t_1. In contrast, the lithium sulfate monohydrate spectrum in Fig. 5b, which also uses a small number of samples, is very narrow and free of truncation artifacts. The inclusion of samples at long evolution times has guaranteed that the linewidth is accurate and that a tightly spaced doublet was not missed, a danger that has been highlighted already in Fig. 2. Given that the barium chlorate and lithium sulfate samples have identical quadrupole parameters, the nonlinear sampling methodology has permitted the acquisition of large numbers of transients for a small number of slices while avoiding truncation artifacts. The sensitivity of the lithium sulfate spectrum is good and we estimate that quadrupole couplings as large as $e^2qQ/h = 8.0$ MHz could be studied at 9.4 T with nonlinear methods. This is supported also by our ability to record the L-asparagine spectrum in Fig. 5a, in which sensitivity was also hindered by high proton density and dehydration. Satisfactory acquisition of this spectrum depended critically upon nonlinear sampling and MaxEnt reconstruction, which permitted recording samples with long evolution times necessitated by the possibility that there may be slight non-degeneracy in the water positions. Indeed the use of NMR-observed quadrupole coupling parameters to refine crystal structures is already known [93]. However, Fig. 5a supports the equivalence of all six water molecules in the unit cell of L-asparagine monohydrate [91,92].

Noisy or severely truncated data invariably degrade the quality of spectral estimates, and different spectral estimation techniques manifest this degradation in different ways. For example, the DFT introduces Gibbs oscillations, or sinc-wiggles, when applied to truncated data. LP and related methods such as FDM avoid truncation artifacts, but may introduce spurious peaks or bias the estimates of peak parameters such as the frequency or phase [44]. The spectra of $(NH_4H_2P^{17}O_4)$ in Fig. 4 illustrate the defects that can appear in MaxEnt spectra of noisy, sparsely sampled data. While the isotropic line position in f_1 and corresponding anisotropic broadening in f_2 are consistent for all processing and sampling schemes in Fig. 4, the isotropic line obtained from 16 t_1 slices by MaxEnt (bottom panel) is slightly broadened near the baseline, unlike the spectrum obtained from the full dataset (48 t_1 slices) by Fourier transformation (top panel). This behavior is also apparent in Fig. 5, where the spectrum of L-asparagine monohydrate has a higher noise level than the lithium sulfate spectrum. The broadening of peaks in MaxEnt spectra that occurs with noisy or truncated data is a direct consequence of maximizing the entropy in the face of weaker experimental constraints on the true lineshape. However, the drawbacks of the minor distortions in the lineshapes are more than outweighed by the benefit of improved resolution possible with nonlinear sampling and MaxEnt reconstruction.

A promising direction for solid-state spectroscopy is the acquisition of two-dimensional experiments in real time, in which the traditional approach of acquiring t_1 slices consecutively would be replaced by acquiring full 2D-MQMAS spectra consecutively. Acquiring full n-D data in real time provides the spectroscopist with valuable feedback: one can monitor the experiment and halt it when the desired sensitivity has been achieved, and unsatisfactory resolution can be detected earlier since slice-wise acquisition does not report on the resolution until the last slice is completed. The decreased number of t_1 samples afforded by MaxEnt reconstruction of

nonlinearly sampled data should enable real-time acquisition of full, phase-sensitive MQMAS spectra.

6. Conclusion

We have used MaxEnt reconstruction to obtain accurate and sensitive nonlinearly sampled ^{17}O 3Q-MQMAS spectra in one and two dimensions. We find that time-savings of factors of 2–4 may be realized and invested in acquiring additional transients if needed. Alternatively, the time-savings may be useful in the implementation of 3D experiments, which are beginning to emerge in quadrupolar applications [41,94]. A distinct advantage of using nonlinear sampling is the ability to record samples at long times so that the full potential of the MQMAS experiment to provide narrow, isotropic lines can be realized.

We find MaxEnt reconstruction to be robust and straightforward to use, particularly since no assumptions regarding the shape or number of resonances are required. When processing the phase-sensitive, two-dimensional MQMAS experiment, MaxEnt was able to retain accurate quadrupole broadened lineshapes in the kilohertz regime in f_2 and provide resolved isotropic lines in the sub-kilohertz regime in f_1. MaxEnt is thus well-suited for wider application in multi-dimensional solid-state NMR.

7. Experimental

Solid-state ^{17}O spectra were acquired on a Cambridge Instruments spectrometer operating at 9.4 T ($\nu_0(^{17}O) = 53.924$ MHz). A custom built, double channel probe employing a Chemagnetics 3.2 mm spinning assembly (Varian Instruments, Fort Collins, CO) was used for all experiments and routinely achieved r.f. irradiation powers of $\nu_{rf}(^{17}O) = 125$ kHz and $\nu_{rf}(^{1}H) > 100$ kHz. For all experiments, magic-angle spinning frequencies were regulated with a Bruker controller (Bruker, Billerica, MA) at $\nu_{MAS} = 19.8 \pm 0.05$ kHz for rotor-synchronization of the evolution period. The indirect dimension was incremented in steps of $\Delta t_1 = 12.5\,\mu s$ (Fig. 2) or $\Delta t_1 = 50.5\,\mu s$ (Figs. 3–5), yielding MQMAS spectral widths of $1/(1+k)\Delta t_1 = 30.97$ or $1/(1+k)\,\Delta t_1 = 7.67$ kHz, respectively. All ^{17}O chemical shifts are reported relative to liquid $H_2{}^{17}O$ (34%).

^{17}O-enriched hydroxyapatite, $Ca_5(P^{17}O_4)_3(OH)$, and ammonium dihydrogen phosphate, $NH_4H_2P^{17}O_4$, were obtained by literature methods [95–97]. The Li_2SO_4-$H_2{}^{17}O$ and L-asparagine monohydrate ($H_2{}^{17}O$) sample were obtained by recrystallizing from 74% ^{17}O-enriched water at room temperature, which is recovered under vacuum. ^{17}O-enriched water was purchased from ISOTEC (Miamisburg, OH).

Data processing was carried out in the RNMRP processing environment (D. Ruben, MIT/Harvard Center for Magnetic Resonance, Cambridge, MA) and the Rowland NMR Toolkit (A. Stern, J. Hoch, Rowland Inst. for Science, Cambridge, MA). The Rowland NMR Toolkit includes the implementation of the MaxEnt reconstruction algorithm and was used to process all nonlinearly sampled data. Simulations of quadrupole lineshapes were carried out in the GAMMA simulation environment [98] using conventional density operator propagation and also a Floquet approach for efficient simulation of MAS sideband spectra [93]. Two-dimensional pure absorption mode spectra were obtained by the hypercomplex method [99]. After two phase-shifted datasets are acquired, they may be appropriately combined to yield echo and anti-echo signals. The latter should contain no signal since this pathway does not allow for refocusing of second-order terms in spin space. Each slice of the 2D echo dataset is treated with an appropriately shifted Gaussian window function before the first Fourier transform along t_2. A t_1-dependent phase correction is then applied to each slice to correct for the time-shifted echo before the spectrum is processed either by FT or MaxEnt along t_1. Alternatively, the t_1-dependent phase correction may be replaced by performing a t_1-dependent rotation of each slice before the first Fourier transform along t_2. Some phasing of the final 2D spectrum may be needed.

Acknowledgments

We are grateful to Dr. David Ruben for insight into the treatment of these datasets and to Dr. Tony Bielecki for several helpful discussions. Dr. Marc Baldus and Dr. Scott Smith provided many important suggestions for the use of GAMMA. This work has built upon prior ^{17}O MQMAS work by Dr. Gang Wu and sample preparation was assisted by Philip Huang. We gratefully acknowledge the support of the Rowland Institute for Science (J.H. and A.S.), the National Institutes of Health Grants GM23403 and RR00995 (B.I., C.F., and R.G.G.), GM47467 (D.R., G.W., J.H., and A.S.), CA89940 (D.R.), and the National Science Foundation, MCB-9316938 (D.R., G.W., J.H., and A.S.).

References

[1] W. Saenger, in: C.R. Cantor (Ed.), Principles of Nucleic Acid Structure, Springer Advanced Texts in Chemistry, Springer, New York, NY, 1984.
[2] S.J. Lippard, J.M. Berg, Principles of Bioinorganic Chemistry, University Science Book, Mill Valley, CA, 1994.
[3] H. He, J. Klinowski, G. Saba, M. Casu, A. Lai, ^{23}Na NMR studies of Na–DNA in the solid state, Solid State Nucl. Magn. Reson. 10 (1998) 169–175.

[4] D. Rovnyak, M. Baldus, G. Wu, N. Hud, J. Feigon, R.G. Griffin, Localization of ^{23}Na+ in a DNA quadruplex by high-field solid state NMR, J. Am. Chem. Soc. 122 (2000) 11423–11429.
[5] A. Medek, V. Frydman, L. Frydman, ^{59}Co NMR studies of diamagnetic porphyrin complexes in the solid phase, J. Phys. Chem. B 101 (44) (1997) 8959–8966.
[6] A. Medek, V. Frydman, L. Frydman, Solid and liquid phase ^{59}Co NMR studies of cobalamins and their derivatives, Proc. Natl. Acad. Sci. USA 94 (1997) 14237–14242.
[7] A. Wong, G. Wu, Solid-state ^{23}Na nuclear magnetic resonance of sodium complexes with crown ethers, cryptands, and naturally occurring antibiotic ionophores: a direct probe to the sodium binding sites, J. Phys. Chem. A 104 (2000) 11844–11852.
[8] C.V. Grant, V. Frydman, J.S. Harwood, L. Frydman, ^{59}Co solid-state NMR as a new probe for elucidating metal binding in polynucleotides, J. Am. Chem. Soc. 124 (2002) 4458–4462.
[9] S. Sham, G. Wu, Solid-state ^{25}Mg NMR study of inner-sphere Mg(2+) binding complexes, Inorg. Chem. 39 (2000) 4–5.
[10] G. Wu, Zinc-67 nuclear magnetic resonance spectroscopy of solids, Chem. Phys. Lett. 298 (1998) 375–380.
[11] F. Larsen, A.S. Lipton, H.J. Jakobsen, N.C. Nielsen, P.D. Ellis, ^{67}Zn QCPMG solid-state NMR studies of zinc complexes as models for metalloproteins, J. Am. Chem. Soc. 121 (1999) 3783–3784.
[12] S. Dong, R. Ida, G. Wu, A combined experimental and theoretical ^{17}O NMR study of crystalline urea: an example of large hydrogen-bonding effects, J. Phys. Chem. A 104 (2000) 11194–11202.
[13] K. Yamada, S. Dong, G. Wu, Solid-state ^{17}O NMR investigation of the carbonyl oxygen electric-field-gradient tensor and chemical shielding tensor in amides, J. Am. Chem. Soc. 122 (2000) 11602–11609.
[14] E. Oldfield, H.C. Lee, C. Coretsopoulos, F. Adebodun, K.D. Park, S. Yang, J. Chung, B. Phillips, Solid-state oxygen-17 nuclear magnetic resonance spectroscopic studies of (17-O_2) picket fence porphyrin, myoglobin, and hemoglobin, J. Am. Chem. Soc. 113 (1991) 8680–8685.
[15] M.T. McMahon, A.C. deDios, N. Godbout, R. Salzmann, D.D. Laws, H. Le, R.H. Havlin, E. Oldfield, An experimental and quantum chemical investigation of CO binding to heme proteins and model systems: a unified model based on ^{13}C, ^{17}O, and ^{57}Fe nuclear magnetic resonance and ^{57}Fe Mossbauer and infrared spectroscopies, J. Am. Chem. Soc. 120 (1998) 4784–4797.
[16] R. Salzmann, M. Kaupp, M.T. McMahon, E. Oldfield, Solid-state nuclear magnetic resonance spectroscopic and quantum chemical investigation of ^{13}C and ^{17}O chemical shift tensors, ^{17}O nuclear quadrupole coupling tensors, and bonding in transition–metal carbonyl complexes and clusters, J. Am. Chem. Soc. 120 (1998) 4771–4783.
[17] R. Salzmann, C.J. Ziegler, N. Godbout, M.T. McMahon, K.S. Suslick, E. Oldfield, Carbonyl complexes of Iron(II), Ruthenium(II), and Osmium(II) 5,10,15,20-tetraphenylporphyrinates: a comparitive investigation by X-ray crystallography, solid-state NMR spectroscopy, and density functional theory, J. Am. Chem. Soc. 120 (1998) 11323–11334.
[18] A.S. Lipton, M.D. Smith, R.D. Adams, P.D. Ellis, 67-Zn solid-state and single-crystal NMR spectroscopy and X-ray crystal structure of zinc formate dihydrate, J. Am. Chem. Soc. 124 (3) (2002) 410–414.
[19] A.S. Lipton, G.W. Buchko, J.A. Sears, M.A. Kennedy, P.D. Ellis, 67-Zn solid-state NMR spectroscopy of the minimal DNA binding domain of human nucleotide excision repair protein XPA, J. Am. Chem. Soc. 123 (2001) 992–993.
[20] L. Frydman, J.S. Harwood, Isotropic spectra of half-integer quadrupolar spins from bidimensional magic-angle spinning NMR, J. Am. Chem. Soc. 117 (1995) 5367–5368.
[21] A. Medek, J.S. Harwood, L. Frydman, Multiple-quantum magic-angle spinning NMR: a new method for the study of quadrupolar nuclei in solids, J. Am. Chem. Soc. 117 (51) (1995) 12779–12787.
[22] A.P.M. Kentgens, A practical guide to solid-state NMR of half-integer quadrupolar nuclei with some application to disordered systems, Geoderma 80 (1997) 271–306.
[23] J.-P. Kintzinger, in: P. Diehl, E. Fluck, R. Kosfeld (Eds.), Oxygen NMR Characteristic Parameters and Applications, NMR Basic Principles and Progress, Springer, Berlin, 1981, pp. 1–64.
[24] W.G. Klemperer, ^{17}O-NMR spectroscopy as a structural probe, Angew. Chem. Int. Ed. Engl. 17 (1978) 246–254.
[25] C.P. Grey, A.P.A.M. Eijkelenboom, W.S. Veeman, N-14 population transfers in 2-dimensional C-13–N-14–H-1 triple-resonance magic-angle-spinning nuclear magnetic resonance spectroscopy, Solid State Nucl. Magn. Reson. 4 (1995) 113–120.
[26] S. Kuroki, A. Takahashi, I. Ando, A. Shoji, T. Ozaki, Hydrogen-bonding structural study of solid peptides and polypeptides containing a glycine residue by ^{17}O NMR spectroscopy, J. Mol. Struct. 323 (1994) 197–208.
[27] K. Yamauchi, S. Kuroki, I. Ando, T. Ozaki, A. Shoji, ^{17}O NMR chemical shifts and quadrupole coupling constants in solid poly(L-alanine)s determined using a high-speed MAS technique, Chem. Phys. Lett. 302 (1999) 331–336.
[28] L.G. Butler, T.L. Brown, Nuclear quadrupole coupling constants and hydrogen bonding. A molecular orbital study of oxygen-17 and deuterium field gradients in formaldehyde–water hydrogen bonding, J. Am. Chem. Soc. 103 (1981) 6541–6549.
[29] R. Goc, E. Ponnusamy, J. Tritt-Goc, D. Fiat, ^{17}O NMR studies of amino acids in the solid state, in single- and polycrystalline forms, Int. J. Pep. Prot. Res. 31 (1988) 130–136.
[30] G. Wu, D. Rovnyak, P.C. Huang, R.G. Griffin, High-resolution oxygen-17 NMR spectroscopy of solids by multiple-quantum magic-angle-spinning, Chem. Phys. Lett. 277 (1997) 79–83.
[31] M.M. Maricq, J.S. Waugh, Rotational spin echoes and high resolution NMR in powders, Chem. Phys. Lett. 47 (1977) 327–329.
[32] G. Wu, D. Rovnyak, R.G. Griffin, Quantitative multiple-quantum magic-angle spinning NMR spectroscopy of quadrupolar nuclei in solids, J. Am. Chem. Soc. 118 (39) (1996) 9326–9332.
[33] F.H. Larsen, H.J. Jakobsen, P.D. Ellis, N.C. Nielsen, Sensitivity-enhanced quadrupolar-echo NMR of half-integer quadrupolar nuclei. Magnitudes and relative orientations of chemical shielding and quadrupole coupling tensors, J. Phys. Chem. A 101 (1997) 8597–8606.
[34] T. Vosegaard, F.H. Larsen, H.J. Jakobsen, P.D. Ellis, N.C. Nielsen, Sensitivity-enhanced multiple-quantum MAS NMR of half-integer quadrupolar nuclei, J. Am. Chem. Soc. 119 (38) (1997) 9055–9056.
[35] G. Wu, S. Kroeker, R.E. Wasylishen, R.G. Griffin, Indirect spin–spin coupling in multiple-quantum magic-angle-spinning NMR spectra of quadrupolar nuclei, J. Magn. Reson. 124 (1996) 237–239.
[36] G. Wu, K. Yamada, Residual dipolar couplings in MAS and MQMAS NMR spectra of quadrupolar nuclei, Chem. Phys. Lett. 313 (1999) 519–524.
[37] S. Wi, L. Frydman, Residual dipolar couplings between quadrupolar nuclei in high resolution solid state NMR: description and observations in the high field limit, J. Chem. Phys. 112 (7) (2000) 3248–3261.
[38] C. Fernandez, L. Delevoye, J.-P. Amoureux, D.P. Lang, M. Pruski, ^{27}Al{^{1}H} cross polarization triple-quantum magic angle spinning NMR, J. Am. Chem. Soc. 119 (29) (1997) 6858–6862.
[39] S.H. Wang, S.M. De Paul, L.M. Bull, High-resolution heteronuclear correlation between quadrupolar and spin 1/2 nuclei

using multiple-quantum magic-angle spinning, J. Magn. Reson. 125 (1997) 364–368.
[40] M. Baldus, D. Rovnyak, R.G. Griffin, Radio-frequency-mediated dipolar recoupling among half-integer quadrupolar spins, J. Chem. Phys. 112 (13) (2000) 5902–5909.
[41] M. Eden, J. Grinshtein, L. Frydman, High resolution 3D exchange NMR spectroscopy and the mapping of connectivities between half-integer quadrupolar nuclei, J. Am. Chem. Soc. 124 (2002) 9708–9709.
[42] G. Wu, Decoupling-induced recoupling in multiquantum magic-angle-spinning NMR spectra of quadrupolar nuclei, Chem. Phys. Lett. 322 (2000) 513–519.
[43] M. Eden, L. Frydman, Quadrupolar-driven recoupling of homonuclear dipolar interactions in the nuclear magnetic resonance of rotating solids, J. Chem. Phys. 114 (9) (2001) 4116–4123.
[44] A.S. Stern, K.-B. Li, J.C. Hoch, Modern spectrum analysis in multidimensional NMR spectroscopy: comparison of linear-prediction extrapolation and maximum-entropy reconstruction, J. Am. Chem. Soc. 124 (9) (2002) 1982–1993.
[45] J.C. Hoch, A.S. Stern, NMR Data Processing, Wiley-Liss, New York, 1996.
[46] H. Hu, A.A. De Angelis, V.A. Mandelshtam, A.J. Shaka, The multidimensional filter diagonalization method II. Application to 2D projections of 2D, 3D, and 4D NMR experiments, J. Magn. Reson. 144 (2000) 357–366.
[47] V.A. Mandelshtam, The multidimensional filter diagonalization method I. Theory and numerical implementation, J. Magn. Reson. 144 (2000) 343–356.
[48] G. Mali, J.-P. Amoureux, V. Kaucic, ^{27}Al–^{31}P 3QMAS/HETCOR experiment in aluminophosphate molecular sieves, Phys. Chem. Chem. Phys. 2 (2001) 5737–5742.
[49] J.C. Hoch, A.S. Stern, in: D.M. Grant, R.K. Harris (Eds.), Maximum Entropy Reconstruction, Encyclopedia of Nuclear Magnetic Resonance, Wiley, Chichester, 1996, pp. 2980–2988.
[50] R.R. Ernst, Sensitivity enhancement in magnetic resonance, Adv. Magn. Reson. 2 (1966) 1.
[51] P. Schmieder, A.S. Stern, G. Wagner, J.C. Hoch, Application of non-linear sampling to COSY-type spectra, J. Biomol. NMR 3 (1993) 569–576.
[52] P. Schmieder, A.S. Stern, G. Wagner, J.C. Hoch, Improved resolution in triple resonance spectra by nonlinear sampling in the constant-time domain, J. Biomol. NMR 4 (1994) 483–490.
[53] C.E. Shannon, A mathematical theory of communication, Bell Syst. Tech. J. 27 (1948) 379–423.
[54] J.C. Hoch, A.S. Stern, D.L. Donoho, I.M. Johnstone, Maximum entropy reconstruction of complex (phase-sensitive) spectra, J. Magn. Reson. 86 (1990) 236–246.
[55] G.J. Daniell, P.J. Hore, Maximum entropy NMR—a new approach, J. Magn. Reson. 84 (1989) 515–536.
[56] D.L. Donoho, I.M. Johnstone, A.S. Stern, J.C. Hoch, Does the maximum entropy method improve sensitivity?, Proc. Natl. Acad. Sci. USA 87 (1990) 5066–5068.
[57] J. Skilling, R.K. Bryan, Maximum entropy image reconstruction: general algorithm, Mon. Not. R. Astron. Soc. 211 (1984) 111–124.
[58] P. Schmieder, A.S. Stern, G. Wagner, J.C. Hoch, Quantification of maximum-entropy spectrum reconstructions, J. Magn. Reson. 125 (1997) 332–339.
[59] J.-L. Pons, T.E. Malliavin, M.A. Delsuc, GIFA V.4: a complete package for NMR data set processing, J. Biomol. NMR 8 (1996) 445–452.
[60] F. Delaglio, S. Grzesiek, G.W. Vuister, G. Zhu, J. Pfeifer, A. Bax, NMRPipe: a multidimensional spectral processing system based on UNIX pipes, J. Biomol. NMR 6 (1995) 277–293.
[61] W. Boucher, AZARA home page, http://www.bio.com.ac.uk/azara, revised 30 October 2002 (4 February 2003).
[62] A. Abragam, Principles of Nuclear Magnetism, Oxford University Press, Oxford, 1961.
[63] H.W. Spiess, Rotation of Molecules and Nuclear Spin Relaxation, Dynamic NMR Spectroscopy, Springer, Berlin, 1978.
[64] M. Goldman, P.J. Grandinetti, A. Llor, Z. Olejiniczak, J.R. Sacheleben, J.W. Zwanziger, Theoretical aspects of higher-order truncations in solid-state nuclear magnetic resonance, J. Chem. Phys. 97 (1992) 8947–8960.
[65] B.Q. Sun, J.H. Baltisberger, Y. Wu, A. Samoson, A. Pines, Sidebands in dynamic angle spinning (DAS) and double rotation (DOR) NMR, Solid State Nucl. Magn. Reson. 1 (1992) 267–295.
[66] M.E. Rose, Elementary Theory of Angular Momentum, Wiley, New York, 1957.
[67] G. Wu, D. Rovnyak, B. Sun, R.G. Griffin, High-resolution multiple quantum MAS NMR spectroscopy of half-integer quadrupolar nuclei, Chem. Phys. Lett. 249 (1996) 210–217.
[68] J.-P. Amoureux, C. Fernandez, L. Frydman, Optimized multiple-quantum magic-angle spinning NMR experiments on half-integer quadrupoles, Chem. Phys. Lett. 259 (1996) 347–355.
[69] N.C. Nielson, H. Bildsoe, H.J. Jakobsen, Finite RF pulse excitation in MAS NMR of quadrupolar nuclei. Quantitative aspects and multiple-quantum excitation, Chem. Phys. Lett. 191 (1992) 205.
[70] S. Vega, Y. Naor, Triple quantum NMR on spin systems with $I = 3/2$ in solids, J. Chem. Phys. 75 (1) (1981) 75–86.
[71] T. Vosegaard, P. Florian, D. Massiot, P.J. Grandinetti, Multiple quantum magic-angle spinning using rotary resonance excitation, J. Chem. Phys. 114 (10) (2001) 4618–4624.
[72] P. Madhu, A. Goldbourt, L. Frydman, S. Vega, Sensitivity enhancement in MQMAS spectroscopy using fast amplitude modulated pulses, in: 40'th Experimental Nuclear Magnetic Resonance Conference (ENC), Orlando, FL 1999.
[73] A.P.M. Kentgens, R. Verhagen, Advantages of double frequency sweeps in static, MAS and MQMAS NMR of Spin $I = 3/2$ nuclei, Chem. Phys. Lett. 300 (1999) 435–443.
[74] T. Vosegaard, D. Massiot, P.J. Grandinetti, Sensitivity enhancements in MQ-MAS NMR of spin-5/2 nuclei using modulated RF mixing pulses, Chem. Phys. Lett. 326 (2000) 454–460.
[75] H.-T. Kwak, S. Prasad, Z. Yao, P.J. Grandinetti, J.R. Sachleben, L. Emsley, Enhanced sensitivity in RIACT/MQMAS NMR experiments using rotor assisted population transfer, J. Magn. Reson. 150 (2001) 71–80.
[76] A. Goldbourt, P.K. Madhu, S. Vega, Enhanced conversion of triple to single-quantum coherence in the triple-quantum MAS NMR spectroscopy of spin-5/2 nuclei, Chem. Phys. Lett. 320 (2000) 448–456.
[77] D. Rovnyak, M. Baldus, R.G. Griffin, Multiple-quantum cross polarization in quadrupolar spin systems during magic-angle spinning, J. Magn. Reson. 142 (2000) 145–152.
[78] K. Lim, C. Grey, Triple quantum cross-polarization NMR of H-1/Al-27 and F-19/Na-23 spin systems in solids, Chem. Phys. Lett. 312 (1999) 45–56.
[79] S. Ashbrook, S. Brown, S. Wimperis, Multiple-quantum cross-polarization in MAS NMR of quadrupolar nuclei, Chem. Phys. Lett. 288 (1998) 509.
[80] J.-P. Amoureux, C. Fernandez, S. Steuernagel, Z-filtering in MQMAS NMR, J. Magn. Reson. A 123 (1996) 116.
[81] J.C.J. Barna, E.D. Laue, Conventional and exponential sampling for 2D NMR experiments with application to a 2D NMR spectrum of a protein, J. Magn. Reson. 75 (1987) 384–389.
[82] J.C.J. Barna, E.D. Laue, M.R. Mayger, J. Skilling, S.J.P. Worrall, Exponential sampling, an alternative method for sampling in two-dimensional NMR experiments, J. Magn. Reson. 73 (1987) 69–77.
[83] D. Massiot, Sensitivity and lineshape improvements of MQ-MAS by rotor-synchronized data acquisition, J. Magn. Reson. A 122 (1996) 240–244.

[84] C. Fernandez, J.-P. Amoureux, 2D multiquantum MAS-NMR spectroscopy of ^{27}Al in aluminophosphate molecular sieves, Chem. Phys. Lett. 242 (1995) 449–454.
[85] S.J. Vega, Fictitious spin 1/2 operator formalism for multiple quantum NMR, J. Chem. Phys. 68 (1978) 5518–5527.
[86] A. Wokaun, R.R. Ernst, Selective excitation and detection in multilevel spin systems: application of single transition operators, J. Chem. Phys. 67 (1977) 1752–1758.
[87] A.J. Vega, MAS NMR spin locking of half-integer quadrupolar nuclei, J. Magn. Reson. 96 (1992) 50–68.
[88] S.P. Brown, S. Wimperis, Two-dimensional multiple-quantum MAS NMR of quadrupolar nuclei: a comparison of methods, J. Magn. Reson. A 128 (1997) 42–61.
[89] D. Iuga, A.P.M. Kentgens, Triple-quantum excitation enhancement in MQMAS experiments on spin $I = 5/2$ systems, Chem. Phys. Lett. 343 (2001) 556–562.
[90] L. Chopin, S. Vega, T. Gullion, A MAS NMR method for measuring ^{13}C–^{17}O distances, J. Am. Chem. Soc. 120 (1998) 4406–4409.
[91] W.D. Arnold, L.K. Sanders, M.T. McMahon, A.V. Volkov, G. Wu, P. Coppens, S.R. Wilson, N. Godbout, E. Oldfield, Experimental, Hartree–Fock, and density functional theory investigations of the charge density, dipole moment, electrostatic potential, and electric field gradients in L-asparagine monohydrate, J. Am. Chem. Soc. 122 (2000) 4708–4717.
[92] M. Ramanadham, S.K. Sikka, R. Chidambaram, Structure of L-asparagine monohydrate by neutron diffraction, Acta Cryst. B 28 (1972).
[93] M. Baldus, B.H. Meier, R.R. Ernst, A.P.M. Kentgens, H. Meyer zu Altenschildesche, Structure investigation on anhydrous disodium hydrogen phosphate using solid-state NMR and X-ray techniques, J. Am. Chem. Soc. 117 (1995) 5141–5147.
[94] S. Wi, H. Heise, A. Pines, Reintroducing anisotropic interactions in magic-angle-spinning NMR of half-integer quadrupolar nuclei: 3D MQMAS, J. Am. Chem. Soc. 124 (2002) 10652–10653.
[95] A. Perloff, A.S. Posner, Preparation of pure hydroxyapatite crystals, Science 124 (1956) 583.
[96] D.G. Ott, Syntheses with Stable Isotopes of Carbon, Nitrogen, and Oxygen, Wiley, New York, 1981.
[97] T.H. Walter, G.L. Turner, E. Oldfield, Oxygen-17 cross-polarization NMR spectroscopy of inorganic solids, J. Magn. Reson. 76 (1988) 106–120.
[98] S.A. Smith, T.O. Levante, B.H. Meier, R.R. Ernst, Computer simulations in magnetic resonance. An object oriented programming approach, J. Magn. Reson. A 106 (1994) 75.
[99] D. Massiot, B. Touzo, D. Trumeau, J.P. Coutures, J. Virlet, P. Florian, P.J. Grandinetti, Two-dimensional magic-angle spinning isotropic reconstruction sequences for quadrupolar nuclei, Solid State Nucl. Magn. Reson. 6 (1996) 73–83.
[100] G.J. Bowden, W.D. Hutchison, J. Khachan, Tensor operator formalism for multiple-quantum NMR. 2. Spins 3/2, 2 and 5/2 and General I, J. Magn. Reson. 67 (1986) 415–437.
[101] G.J. Bowden, W.D. Hutchison, Tensor operator formalism of multiple-quantum NMR. 1. Spin-1 nuclei, J. Magn. Reson. 67 (1986) 403–414.